

Article

Role of *N*-Oxide Moieties in Tuning Supramolecular Gel-State Properties

Dipankar Ghosh ¹, Ragnar Bjornsson ² and Krishna K. Damodaran ^{1,*}

¹ Department of Chemistry, Science Institute, University of Iceland, Dunhagi 3, 107 Reykjavík, Iceland; dig11@hi.is

² Department of Inorganic Spectroscopy, Max-Planck-Institut für Chemische Energiekonversion, Campus de Stiftstrasse 34–36, 45470 Mülheim an der Ruhr, Germany; ragnar.bjornsson@gmail.com

* Correspondence: krishna@hi.is; Fax: +354-552-8911

Received: 26 October 2020; Accepted: 17 November 2020; Published: 20 November 2020



Abstract: The role of specific interactions in the self-assembly process of low molecular weight gelators (LMWGs) was studied by altering the nonbonding interactions responsible for gel formation via structural modification of the gelator/nongelator. This was achieved by modifying pyridyl moieties of bis(pyridyl) urea-based hydrogelator (**4-BPU**) and the isomer (**3-BPU**) to pyridyl *N*-oxide compounds (**L₁** and **L₂**, respectively). The modification of the functional groups resulted in the tuning of the gelation properties of the parent gelator, which induced/enhanced the gelation properties. The modified compounds displayed better mechanical and thermal stabilities and the introduction of the *N*-oxide moieties had a prominent effect on the morphologies of the gel network, which was evident from the scanning electron microscopy (SEM) images. The effect of various interactions due to the introduction of *N*-oxide moieties in the gel network formation was analyzed by comparing the solid-state interactions of the compounds using single crystal X-ray diffraction and computational studies, which were correlated with the enhanced gelation properties. This study shows the importance of specific nonbonding interactions and the spatial arrangement of the functional groups in the supramolecular gel network formation.

Keywords: LMWGs; hydrogen bonding; pyridyl urea; *N*-oxide; structural modification; computational calculations; stimuli-responsive

1. Introduction

Gels are fascinating semi-solid materials with unique physical characteristics which can retain their solid-like shape but display fluid-like properties on applying external stress [1]. Supramolecular gels based on low molecular weight gelators (LMWGs) [2–7] are materials with intriguing potential applications [5,6,8–12] such as sensing, catalysis, tissue engineering, drug delivery and as a media to control crystal growth. LMWGs offer several advantages over the conventional polymer gels due to their synthetic accessibility, tunable gel state property, inherent reversibility, and smart response towards external stimuli [3–5,13]. LMWGs are formed by the self-assembly of small molecules in the presence of solvents via various nonbonding interactions resulting in the formation of a three-dimensional superstructure with entrapped solvent molecules [2–6,14]. The principles of supramolecular chemistry helped researchers to understand the importance of nonbonding interactions and functional groups in designing LMWGs resulting in a myriad of LMWGs over the past decade with different functional groups [15–24]. However, the dynamic nature of the nonbonding interactions in LMWGs makes it difficult to predict the gel network formation, which is one of the reasons that the discovery of the majority of new LMWGs is serendipitous. Thus, the design of new LMWGs with predictable properties is still challenging because the geometry and spatial arrangement of the building blocks or functional

groups dictate the properties and structure of LMWGs. The effect of various functional groups in the self-assembly process of LMWGs can be analyzed by comparing the gelation properties of LMWGs with similar structures, which will provide a better understanding of the self-assembly process.

An excellent strategy is to modify a well-known gelator comprising supramolecular synthons or hydrogen bonding moieties, which will enable us to compare the gelation and structural properties of the modified gelator with the parent gelator [25]. McNeil et al. have modified an azosulfonate gelator scaffold to develop a nitrite sensor based on LMWGs [26]. We have shown that the modification of the functional group of trimesic amide based gelator N^1, N^3, N^5 -tri(pyridin-3-yl)benzene-1,3,5-tricarboxamide [27] resulted in a *tris-N-oxide* compound with different gelation properties [28]. We have studied the importance of functional groups and the role of nonbonding interactions in tuning gelation properties of LMWGs by altering the intermolecular interactions. This was achieved by modifying the pyridyl groups of *N*-(4-pyridyl)isonicotinamide (4PINA) [29] to *N-oxide* groups, which resulted in two mono-*N-oxide*s and a di-*N-oxide* compound [30]. The strong and unidirectional $N-H\cdots N$ interactions of the parent gelator was disrupted by the modification of the pyridyl group and the effect of these interactions on the gelation properties was studied.

The tuning of gelation properties by functional group modification prompted us to explore this strategy to urea-based pyridyl compounds because urea and amide moieties are extensively used to generate LMWGs [19,31]. Generally, in urea-based LMWGs, the urea motifs self-assemble via complementary hydrogen bonding ($N-H\cdots O=C$) into one-dimensional arrays of hydrogen bonded chain to form α -tapes (fibrils) and the aggregation of these fibrils results in an entangled three-dimensional framework. The solid-state structural analysis of the gelators using single crystal X-ray diffraction (SCXRD) will provide information about the key interactions in the solid-state structure of LMWGs [29,32–38], which can be correlated to the interactions and the packing modes of these molecules in the gel state. The hydrogen-bonding synthons in these LMWGs are strongly influenced by the adjacent functional groups; for example, attaching pyridyl group to urea or amide moiety alters the intermolecular interactions resulting in an $N-H\cdots N$ hydrogen bonding synthon involving the urea/amide group and pyridyl moiety [29,39]. Steed et al. reported that $N-H\cdots N$ interactions also play an important role in the crystal structure of pyridyl-urea compounds [40,41]. These $N-H\cdots N$ interactions can be replaced with $N-H\cdots O$ interactions, which will enable us to study the effect of structural modification and the role of the resulting interaction in the supramolecular gelation of bis(pyridyl)urea compounds. We have selected *N,N'*-bis(3-pyridyl) urea (**3-BPU**) and *N,N'*-bis(4-pyridyl) urea (**4-BPU**) as the parent compounds [32] and the pyridyl nitrogen atoms of **3-BPU/4-BPU** were oxidized to corresponding *N-oxide*s. The structural modification induced gelation or enhanced gelation properties were studied by analyzing the key nonbonding interactions of the parent and modified compounds.

2. Results and Discussion

2.1. Design and Synthesis

The reaction of 4-aminopyridine/3-aminopyridine with triphosgene in the presence of triethylamine in anhydrous dichloromethane resulted in *N,N'*-bis(4-pyridyl) urea (**4-BPU**)/*N,N'*-bis(3-pyridyl) urea (**3-BPU**) [32]. The **3-BPU** did not form hydrogels in pure water and the majority of aqueous solutions whereas **4-BPU** formed gels in water/aqueous solutions and the structural details of **4-BPU** interacting with the gelling solvents has been reported [32]. The structural modifications of the bis(pyridyl) urea compounds were achieved by oxidizing the pyridyl groups of **4-BPU** and **3-BPU** to pyridyl *N-oxide* moieties using 3-chloroperoxybenzoic acid, resulting in di-*N-oxide* urea 4,4'-(carbonylbis(azanediyl))bis(pyridine 1-oxide) (**L₁**) and 3,3'-(carbonylbis(azanediyl))bis(pyridine 1-oxide) (**L₂**), respectively (Scheme 1).

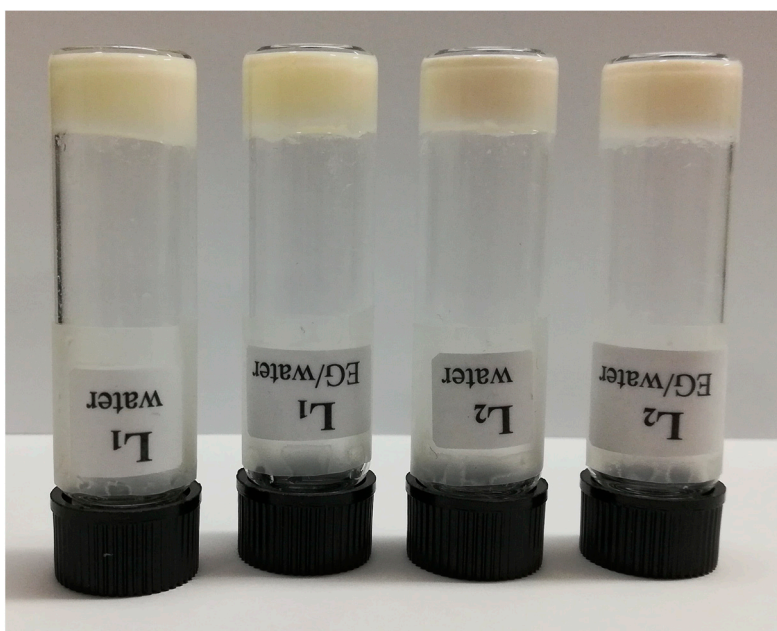


Figure 1. L₁ and L₂ gels obtained from water and EG/water (3:7 *v/v*) mixture.

The minimum gel concentration (MGC) of L₁ was determined by varying the concentration of gelator and the MGC was found to be 0.7 wt% in both water (Table S2) and EG/water mixture (3:7, *v/v*). The MGC of the parent 4-BPU gelator was found to be 0.8 wt% in water and 0.7 wt% in EG/water mixture (3:7, *v/v*). These results clearly indicated that 4-BPU and the modified compound L₁ can form the entangled network, which showed the important role of urea moieties in gel formation. We have also tested the gelation properties of L₂, which was synthesized by modifying 3-BPU. The solubility of L₂ was higher compared to L₁ in water or an aqueous solution of organic solvents. The ability of L₂ to form hydrogel was tested by dissolving 10.0 mg of L₂ in 1.0 mL solvent by heating and sonicating, and the solution was left undisturbed. Interestingly, the hydrogel was obtained within an hour (Table 1) and the MGC of L₂ in water was found to be 0.8 wt% (Table S2). Thus, replacing the pyridyl groups with *N*-oxide groups induced hydrogel formation in L₂, which was not observed in parent 3-BPU. The gelation experiments performed in (1:1, *v/v*) aqueous solutions of highly polar solvents (EG, DME, DMF, DMA, DMSO, MeOH, EtOH, MeCN and THF) at 1.0 wt% resulted in gelation of L₂ in all cases. The MGC of L₂ in the EG/water mixture (3:7, *v/v*) was found to be 1.1 wt%. We have also performed gelation experiments by varying the concentration of ethylene glycol and the results showed that increasing the concentration of EG in the EG/water mixture increased the MGC of L₂ gels, indicating that EG acts as the solubilizing agent.

The thermal stabilities of the gel networks were evaluated by gel-to-solution transition temperature (T_{gel}) experiments. The thermal stabilities of 4-BPU, 3-BPU, L₁, and L₂ were measured in water and various EG/water ratios, and the results are summarized in Table 2. The T_{gel} comparison of 4-BPU and L₁ revealed that both the networks displayed similar thermal stabilities in pure water. However, increasing the EG concentration resulted in reduced thermal stability for all the gelators, which may be attributed to the higher solubility of the gelators in EG. The analysis of the thermal stabilities at various solvent compositions showed that L₁ displayed enhanced thermal stabilities compared to 4-BPU (Table 2). The T_{gel} comparison of 3-BPU and L₂ clearly indicate that the thermal stability of the L₂ network is much higher compared to 3-BPU. Furthermore, L₂ is capable of forming gel in a wide range of solvent compositions. Thus, modifying the pyridyl groups of bis(pyridyl) urea compounds have a prominent effect on the thermal stability of the gel network.

Table 2. T_{gel} (°C) comparison of 4-BPU and L₁ at 1.0 wt%, and 3-BPU and L₂ at 2.5 wt% in water and various EG/water ratios.

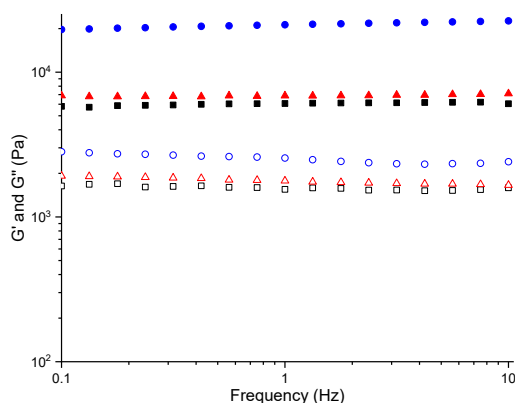
Water: EG	4-BPU *	L ₁ *	3-BPU **	L ₂ **
10:0	98.1	95.2	Crystal	88.2
9:1	85.6	94.5	Crystal	83.6
8:2	81.2	91.7	57.1	79.1
7:3	74.0	91.0	56.4	74.5
6:4	71.6	89.4	Crystal	72.3
5:5	69.5	84.1	Crystal	71.0

* 1.0 wt% and ** 2.5 wt%.

2.3. Rheology

The structural characteristics of the bis(pyridyl) and bis(pyridyl-*N*-oxide) urea gels were analyzed by rheology, which enabled us to compare the relative stiffness or elasticity of the gel networks. The 4-BPU, L₁ and L₂ gels were prepared at 1.0 wt% in water, and the linear viscoelastic region (LVR) was determined by oscillatory strain-sweep experiments, where the elastic modulus (G') was constant irrespective of the shear stress. The experiments were performed within the LVR to ensure that the gel networks underwent reversible deformation, which would enable us to estimate the actual characteristics of the materials. The 4-BPU gel displayed quite narrow LVR, and the G' decreased on increasing the shear strain above 0.05% (Figure S1).

In contrast, the L₁ and L₂ gels were more rigid, and the LVR of these gels were stretched to 0.1% (Figure S1). The cross-over point, where the solid-like property of the gel transformed to a liquid-like property was also higher for the L₁ and L₂ gels. These indicate that the *N*-oxide gels are capable of resisting higher applied forces without irreversible deformation compared to the 4-BPU gel. The frequency sweep experiments performed on the gels at 1.0 wt% in water revealed that both of the storage and loss moduli (G' and G'') were independent of frequency, supporting the gel behavior (Figure 2). The 4-BPU and L₁ gels displayed quite similar G' , but the G' of L₂ gel was significantly higher, indicating that the L₂ gel possessed a stronger network with higher mechanical stability. The relative gel strength of 3-BPU and L₂ was also compared by performing rheology on the gels prepared at 2.5 wt% in EG/water (3:7 *v/v*). The strain sweep (Figure S1) and frequency sweep (Figure S2) experiments performed on both gels revealed that L₂ displayed about 1000 times higher G' compared to the parent 3-BPU. The G' and G'' of 3-BPU did not show a constant value at low-frequency range, indicating that the 3-BPU gel network was soft resulting in a weak solid-like network. This is in excellent agreement with the overall gelation properties of the compounds, which suggested that 4-BPU, L₁ and L₂ were efficient hydrogelators but that 3-BPU was a weak gelator.

**Figure 2.** Frequency sweep experiments performed on 4-BPU, L₁ and L₂ gels at 1.0 wt% in water at 25.0 °C at a constant strain of 0.05%. Color codes: G' , 4-BPU (■), G'' , 4-BPU (□), G' , L₁ (▲), G'' , L₁ (△), G' , L₂ (●), G'' , L₂ (○).

2.4. Gel Morphology

The morphologies of **4-BPU**, **3-BPU**, **L₁**, and **L₂** were studied by scanning electron microscopy (SEM). The **4-BPU** (1.0 wt%), **L₁** (1.0 wt%), **3-BPU** (2.5 wt%) and **L₂** (2.5 wt%) gels were prepared from EG/water (3:7, *v/v*). We have also performed the SEM analysis of **L₁** and **L₂** at 1.0 wt% in water and DMSO/water (1:1, *v/v*). The gels were filtered to remove the solvent and dried for two days to prepare the xerogel and the SEM images of the dried gels indicated the presence of various morphologies (needle, fibrous, tape-like and plate).

The **4-BPU** xerogels obtained from EG/water (3:7, *v/v*) displayed a typical fibrous network with thickness ranging from 2.0 to 8.0 μm (Figure 3a). The morphology of **L₁** gels from both EG/water mixture (Figure 3b) and pure water (Figure S3) was slightly different from the parent **4-BPU** gelator. The xerogels of **L₁** displayed needle-like fibers with thickness ranging from 4.0 to 12.0 μm whereas a tape-like fibrous network was observed in **4-BPU**. The xerogel of **L₁** (1.0 wt%) obtained from DMSO/water mixture (1:1, *v/v*) showed a fibrous tape-like morphology with thickness varying from 0.1 to 1.6 μm (Figure S4). The xerogels of **3-BPU** from EG/water (3:7, *v/v*) displayed a fibrous brick-like morphology (Figure 4a) varying from 5.0 to 20.0 μm but a different morphology was observed for **L₂** xerogels in both EG/water (3:7 *v/v*) (Figure 4b) and pure water (Figure S5).

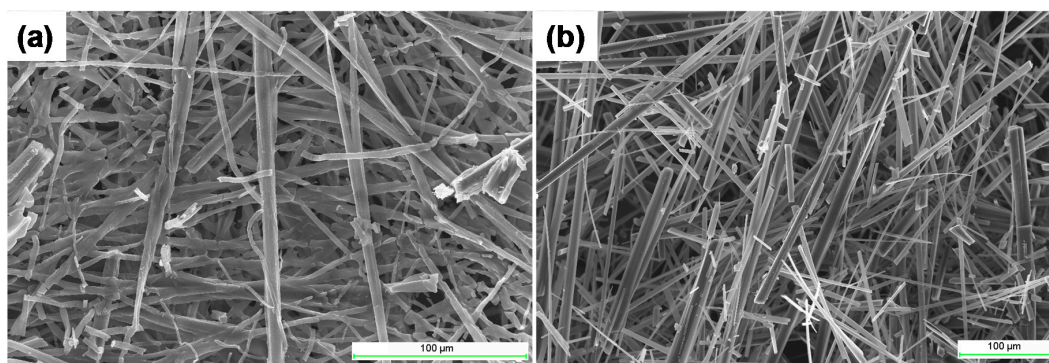


Figure 3. SEM images of (a) **4-BPU** and (b) **L₁** xerogels obtained from EG/water (3:7, *v/v*) at 1.0 wt%.

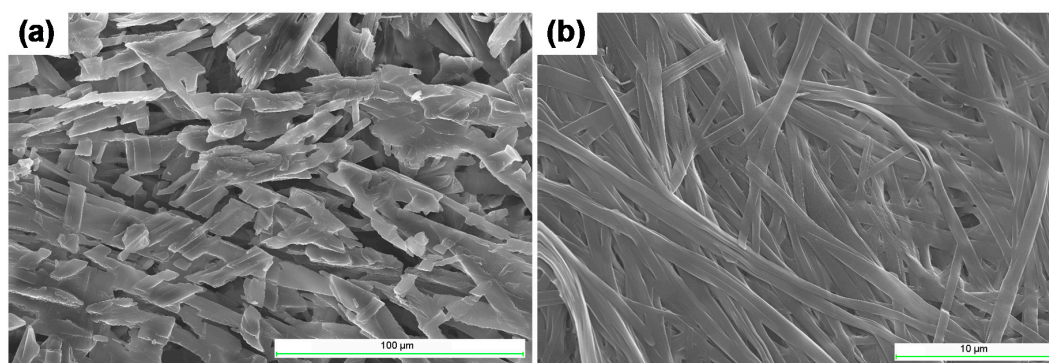


Figure 4. SEM images of (a) **3-BPU** and (b) **L₂** xerogels obtained from EG/water (3:7, *v/v*) at 2.5 wt%.

The thickness of the fibers observed for **L₂** xerogels from EG/water, 3:7 *v/v* and pure water varied from 0.8 to 1.2 μm and 0.2 to 0.8 μm , respectively. The SEM images of **L₂** (1.0 wt%) xerogel obtained from 1:1 DMSO/water mixture (*v/v*) showed morphologies similar to EG/water gels with varying thickness (0.1 to 1.0 μm , Figure S6). These results clearly indicate that modifying the pyridyl group to *N*-oxide groups induced a prominent change in the morphology of the gel fibers. Thus, the mode of intermolecular nonbonding interactions plays an important role in altering the morphology of gel fibers, which prompted us to correlate the solid-state structure of the modified compounds with the parent gelator structure using X-ray diffraction.

2.5. Single Crystal X-ray Diffraction

The solid-state structures of the parent gelator **4-BPU** [32], the isomer **3-BPU** [32], and the *N*-oxide **L₂.H₂O** [42] were compared to the modified **4-BPU** gelator (**L₁**). We were successful in isolating the crystals of the gelators in various solvated forms such as **L₁.H₂O**, **3-BPU.2EG**, and **L₂.EG**. Single crystals of **L₁** were obtained from an aqueous solution of **L₁** below MGC over a period two days. The crystal data and the hydrogen-bonding parameters are summarized in Tables S3 and S4, respectively. Single crystal X-ray diffraction revealed that **L₁** crystallized in a monoclinic space group $P2_1/c$ with one solvent water molecule (**L₁.H₂O**). The molecular plane consisted of one of the pyridyl *N*-oxide moieties and the urea moiety, but the second pyridyl moiety was slightly twisted from the molecular plane (15.6°). The hydrogen bonding modes of the two pyridyl *N*-oxide moieties were different and the twisted pyridyl *N*-oxide moiety displayed N—H \cdots O interaction (2.7990(16) and 2.7851(16) Å) with the urea moiety, which was similar to complementary urea interaction. This interaction resulted in a one-dimensional chain with **L₁** orienting orthogonal to each other displaying urea α -tape-like architecture (Figure 5a). The 1-D chains displayed bifurcated hydrogen bonding with adjacent chains via O—H \cdots O interactions (2.7466(19) and 2.7612(19) Å) involving the planar pyridyl *N*-oxide moiety and the solvent water molecule (Figure 5b).

The analysis of the solid-state structure of **L₁** and the parent gelator (**4BPU**) revealed the absence of complementary N—H \cdots O=C hydrogen bonding motifs in **4BPU** [32] because the pyridyl groups and the urea moieties were hydrogen bonded with the solvent molecules. The structural analysis of the crystals of **L₂** revealed the formation of the solvated form of **L₂** (**L₂.H₂O**) and the unit cell parameters matched with the reported structure [42]. The hydrogen bonding pattern of the pyridyl *N*-oxide and urea moieties of **L₂** was similar to **L₁** and the one-dimensional hydrogen-bonded chain formed was stabilized by the complementary hydrogen bonding [42]. The structure was compared with the parent compound **3-BPU** [32], which existed in two forms (**3-BPU** and **3-BPU.H₂O**). The pyridyl groups of **3-BPU** were involved in N—H \cdots N interactions and these groups were hydrogen bonded to the solvent water molecules in **3-BPU.H₂O** [32]. Thus, replacing the nonbonding interactions resulted in a one-dimensional hydrogen bonded chain in **L₁** and **L₂** stabilized by complementary urea-like hydrogen bonding (N—H \cdots O). Moreover, the alteration of the pyridyl group to the pyridyl *N*-oxide moiety induced gelation resulting in **L₂** hydrogels but the parent **3-BPU** was a nongelator in water.

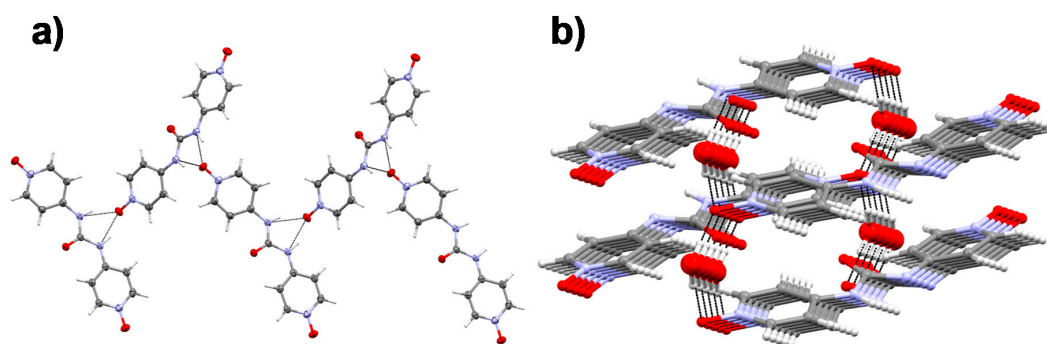


Figure 5. (a) Hydrogen bonded 1-D chain observed in **L₁** and (b) 1-D chains displaying bifurcated hydrogen bonding with adjacent chains and solvent water molecules via O—H \cdots O interactions.

The gelation ability of **3-BPU**, **L₁**, and **L₂** in EG/water prompted us to analyze the crystal structure of these compounds obtained from ethylene glycol. The structural analysis of **3-BPU** obtained from ethylene glycol revealed that **3-BPU** crystallized in monoclinic space group $P2_1/c$ with two EG molecules (**3-BPU.2EG**). The pyridyl nitrogen atoms were oriented trans to each other resulting in an anti-conformation compared to the reported syn-conformation of **3-BPU** and **3-BPU.H₂O** structures [32]. The urea moiety and the pyridyl nitrogen atom of **BPU.2EG** were hydrogen bonded to one of the EG molecules via N—H \cdots O (2.9122(14) and 2.7496(13) Å) and O—H \cdots N (2.7932(15) Å)

interactions resulting in a hydrogen bonded macrocycle (Figure 6a). This macrocycle interacts with adjacent macrocycles via O—H...O interactions (2.7026(15) Å) between the other pyridyl moieties and the second EG molecule to form a two-dimensional hydrogen bonded corrugated sheet-like architecture (Figure 6b). The modified compound L_2 crystallized in an orthorhombic $C222_1$ space group with a formula of $L_2 \cdot EG$ and a syn-conformation of pyridyl N -oxide was observed. One of the N—H groups of the urea moiety interacted with the pyridyl N -oxide group via a complementary urea-like hydrogen bonding (N—H...O = 2.690(2) Å) interaction similar to $L_2 \cdot H_2O$ resulting in a one-dimensional chain (Figure 7a), which interacted with adjacent chains via N—H...O interaction (2.690(2) Å) between the pyridyl N -oxide groups and the other NH groups of the urea moiety. The pyridyl N -oxide moiety also interacted with the EG molecule via O—H...O (2.741(2) Å) hydrogen bonding interaction (Figure 7b) resulting in a three-dimensional hydrogen bonded network.

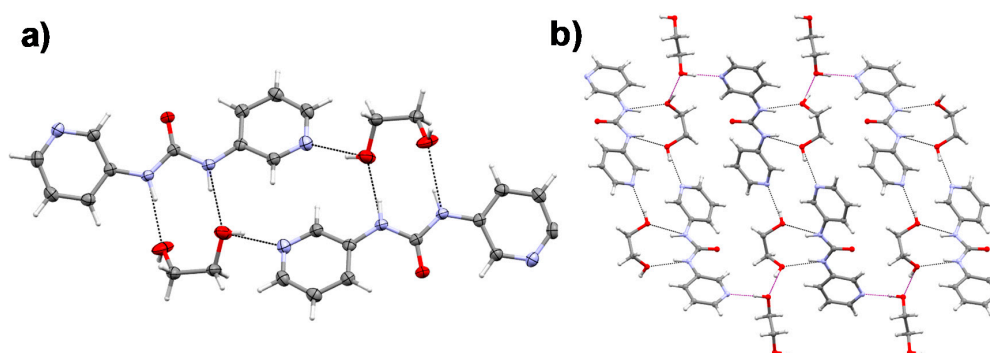


Figure 6. (a) Hydrogen-bonded macrocycle obtained by the interaction of solvent ethylene glycol and BPU molecules in $BPU \cdot 2EG$, (b) macrocycle interacting with adjacent macrocycles via O—H...O interactions.

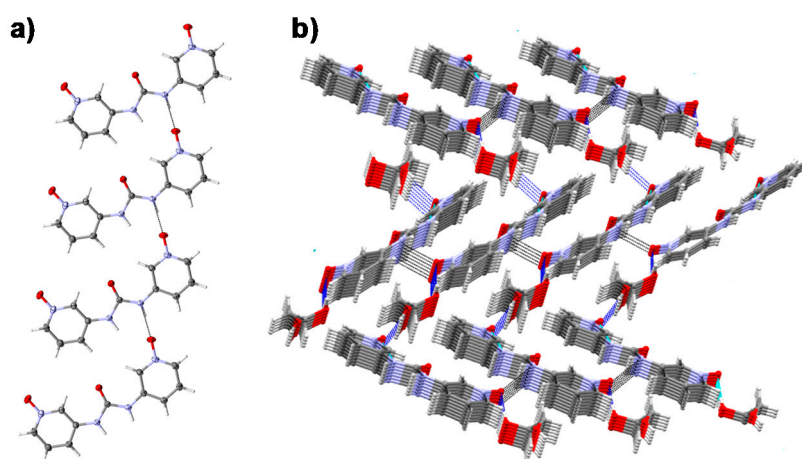


Figure 7. (a) Hydrogen bonded chains in $L_2 \cdot EG$ stabilized by N—H...O interactions between urea and pyridyl N -oxide moieties, (b) one-dimensional chains interacting with adjacent chains via N—H...O interaction involving pyridyl N -oxide groups and the other N—H groups of the urea moiety.

2.6. X-ray Powder Diffraction (XRPD)

The molecular aggregation in the solid-state and gel/dried gel state was compared by the XRPD analysis of the bulk material and the xerogel. We have been successful in identifying the role of various nonbonding interactions in gel formation by comparing the molecular assembly in crystalline and gel/dried gel states [30,43–45]. Although, the xerogel does not represent the exact structure of the gel state since the drying process can lead to a morphological change or phase transition [46], this approach is still recognized as the most useful strategy to unravel the self-assembly of a gelator [3,7,29,30,43–45].

The self-assembly of L_1 and L_2 in the gel state was correlated with respective crystal structures by comparing the powder X-ray pattern of the bulk crystals and dried gels with the crystal structure. The XRPD pattern for the bulk material and xerogel pattern matched with the simulated graph obtained from the single-crystal structure of L_1 (Figure S7). This indicates that the single crystal structure of L_1 truly represents the packing in bulk crystal and the hierarchical xerogel network. We have performed the XRPD of xerogels obtained from water and EG/water mixture (3:7, v/v), and the pattern matched each other but the xerogel pattern obtained from water was less crystalline indicating that EG induced a crystalline nature in gel fibers (Figure S7).

Similar results were observed for L_2 , the XRPD of the L_2 xerogels obtained from EG/water mixture (3:7, v/v) and bulk solid were compared with the simulated pattern of $L_2.H_2O$ and the powder pattern of both bulk crystals and xerogel matched with the simulated pattern of $L_2.H_2O$ (Figure 8). Interestingly, the bulk crystals of $L_2.EG$ from EG did not match the $L_2.EG$ simulated pattern (Figure S8), but matched perfectly with $L_2.H_2O$ pattern, presumably due to the loss of hydrogen bonded EG molecules during the drying process. We observed similar trends for 3-BPU, where XRPD pattern of 3-BPU.EG bulk crystals and xerogels obtained from EG/water mixture (3:7, v/v) showed a perfect match with the simulated 3-BPU pattern (Figure S9) but these patterns were different from the simulated 3-BPU.EG pattern. This confirms the loss of EG molecules in the crystal during the drying process. The xerogel patterns obtained for L_1 and L_2 from water and EG/water mixture (3:7, v/v) indicates that the one-dimensional urea α -tape-like architecture was preserved in the xerogel network.

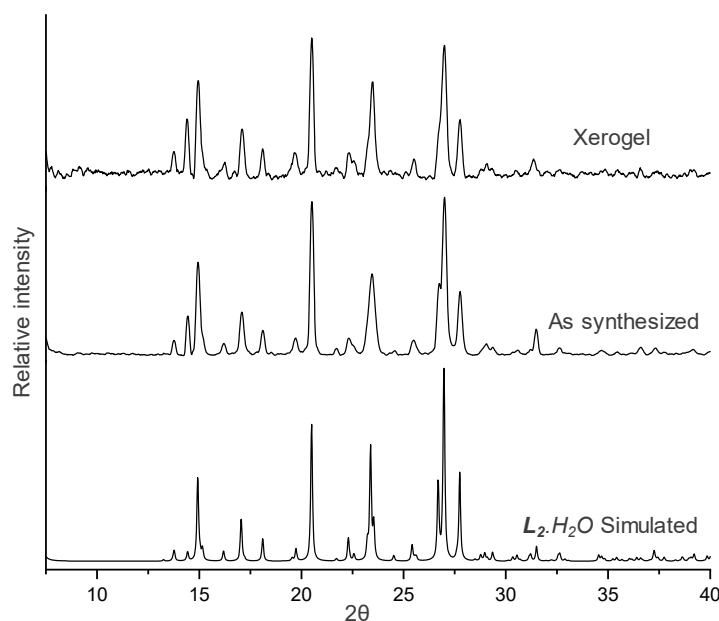


Figure 8. Comparison of the XRPD pattern of simulated, as synthesized and the xerogel from EG/water (3:7 v/v) at 1.2 wt% of L_2 .

2.7. Stimuli-Responsive Property

The amide/urea functionalized LMWGs can be considered as classical stimuli-responsive soft materials due to their response to an external stimulus such as light, redox, pH, and salts/ions [29,37,43,47]. We have shown that the anion responsive properties of supramolecular gels can be used to detect cyanide anions in water by monitoring the gel to sol transition [44]. The stimuli-responsive properties of the gels were studied by treating the hydrogels of 4-BPU, L_1 , and L_2 at 1.0 wt% with different anions such as halides, acetate, and cyanide (sodium or potassium salt), and the relative gel strength of the mixture was compared with the pure gels. The 4-BPU gel was stable with the addition of three equivalents of either fluoride, chloride, bromide, iodide, acetate, and cyanide salts (Figure S10). However, the network was collapsed by the addition of four equivalents of iodide, acetate, and cyanide

ions (Figure 9). The gel was also disrupted by the addition of excess bromide (five equivalents), fluoride (six equivalents), and chloride ions (seven equivalents). This indicates that larger anions were more effective in breaking the gel network, presumably due to the enhanced interactions with the N—H...N hydrogen bonding synthons. The higher efficiency of fluoride in disrupting the gel network compared to the chloride ion may be attributed to the strong hydrogen bonding capability of the fluoride ions. The experiments performed with the modified gelator showed that L_1 was more sensitive to the anions (Figure S11), and the gel was collapsed by the addition of two equivalents of iodide and cyanide ions. The gel network was also collapsed in the presence of three equivalents of bromide and four equivalents of acetate ions (Figure 9). These results clearly indicate that L_1 gel is more responsive compared to the parent 4-BPU gel.

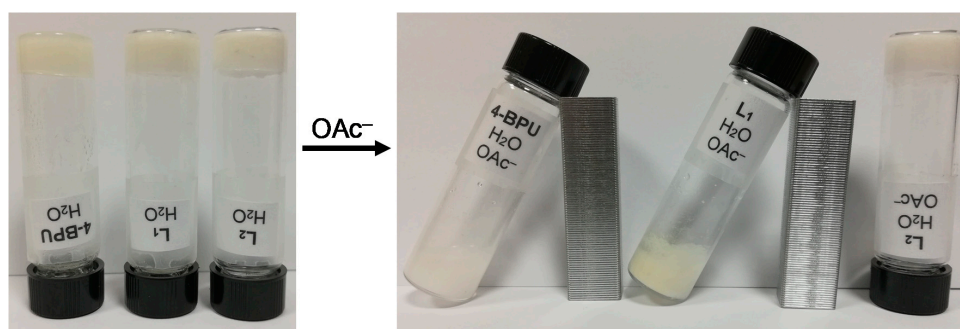


Figure 9. The effect of four equivalents of acetate anion on 4-BPU, L_1 and L_2 gels.

Interestingly, the L_2 hydrogel displayed much higher stability towards anions compared to 4-BPU and L_1 gels, and the gel network was stable even after the addition of six equivalents of anions in all cases. This was due to the rigid network of L_2 compared to 4-BPU and L_1 gels, thus L_2 exhibited more resistance against the anions. The effect of the anions on the gel network was further analyzed by rheology. The addition of three equivalents of anions to the L_2 gel resulted in the reduction of the storage modulus, however, no significant difference in the G' value was observed with various anions (Figure S12). The G' of the gels decreased by increasing the concentration of the anions (six equivalents) for bromide, iodide, acetate, and cyanide ions (Figure 10). The larger ions such as acetate and cyanide showed the lowest G' values for L_2 , which corroborates the experiments with 4-BPU and L_1 gels. The analysis of the anion sensing experiments suggests that the modification of the functional groups can potentially generate gels with higher sensitivity and resistance.

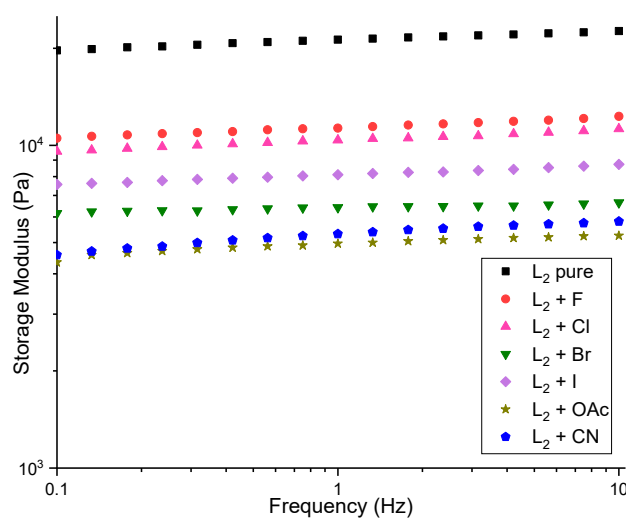


Figure 10. Frequency sweep experiments performed at 25.0 °C at a constant strain of 0.02% on L_2 hydrogel at 1.0 wt%, in the presence of six equivalents of anions.

2.8. Computational Studies

To rationalize these observations, we have calculated the strengths of different hydrogen-bonding interactions using quantum chemical calculations via a state-of-the-art density functional theory (DFT)-based protocol (ω B97M-D3BJ/def2-TZVP). Interactions of gelators/nongelators with themselves as well as with single solvent molecules EG and water molecules were calculated. These calculations performed in the gas phase allowed us to compare the hydrogen-bonding interaction strength of different functional groups, which were not intended, however, to mimic the complex solution/gel environment. Figures S13–S16 (see Supplementary Materials) show the optimized geometries as well as interaction energies. Calculations of the nongelator **3BPU** revealed that the strongest **3BPU** dimer interaction was -17.5 kcal/mol (ΔE) and involved N—H \cdots O hydrogen-bonding. This was almost equal to the **3BPU**–EG interaction of -17.8 kcal/mol. The **4-BPU** dimer can hydrogen-bond via either N—H \cdots O or N—H \cdots N. The stronger N—H \cdots O interaction within the **4-BPU** dimer (-15.4 kcal/mol) was, however, calculated to be weaker than the N—H \cdots O interaction between **4BPU** and EG (-16.6 kcal/mol). The hydrogen-bonding interactions with water and **3-BPU/4-BPU** were generally calculated to be weaker than **3-BPU/4-BPU** dimer interactions but interactions with EG were predicted to be strongest overall.

Calculations of **L₁** and **L₂** dimers revealed a rather different picture. The **L₁–L₁** dimer interaction via N—H \cdots O hydrogen bond was rather a stronger interaction (-19.9 kcal/mol) that can be compared to the relatively weak H₂O–**L₂** O—H \cdots O—N interaction (-10.4 kcal/mol) and the EG–**L₁** N—H \cdots O interaction (-16.6 kcal/mol). For the **L₂–L₂** dimer we found two different conformations. For example, one with an approximately parallel alignment of the **L₂** units and another with more perpendicular alignment. The parallel conformation had the interaction energy of -19.6 kcal/mol while the perpendicular conformation had the interaction energy of -24.3 kcal/mol. Both of these conformations were found to be stronger than **L₂–EG** interactions (-15.1 kcal/mol) and an **L₂·H₂O** interaction (-8.8 kcal/mol). These simple hydrogen-bonding calculations in the gas phase do not explain why **4-BPU** was a gelator and **3-BPU** a non-hydrogelator. More complex calculations that take the solution/gel environment into account are likely required to understand the nature of the gelation process. The increased dimer hydrogen-bonding interaction strength in going from **3-BPU** to **L₂** via pyridyl nitrogen to *N*-oxide substitution is, however, a plausible model for why **L₂** formed the better gels than **3-BPU**.

3. Conclusions

The structural modification of the gelator/nongelator was used as a strategy to alter the nonbonding interactions responsible for gel formation to induce/enhance the gelation properties of LMWGs. This was achieved by converting the pyridyl moieties of a bis(pyridyl) urea-based hydrogelator (**4-BPU**) and a non-hydrogelator (**3-BPU**) to pyridyl *N*-oxides compounds (**L₁** and **L₂**, respectively). The gelation properties of the modified compounds and the parent compounds were analyzed by standard gelation techniques and improved thermal stability was observed for **L₁** compared to the parent **4-BPU**. The hydrogel formation of **L₂** clearly indicates that the structural modification of **3-BPU** induced gelation. The modified gelator **L₂** turned out to be an excellent gelator in water and mixed aqueous solvents. The modification of the functional groups had a prominent effect on the mechanical and thermal stability of the gel network and the modified gelators showed higher sol–gel transition temperatures (T_{gel}). The morphologies of the xerogels were analyzed by comparing the SEM images, which showed that brick-like morphology of **3-BPU** was replaced by an efficient fibrous network in **L₂** in water, which corroborates well with the gelation results. The comparison of the solid-state structures revealed that a one-dimensional chain was formed via N—H \cdots O interaction similar to complementary urea interaction, which was crucial for the formation of the gel network. The enhanced gelation properties resulting from the alteration of N—H \cdots N interaction to N—H \cdots O interaction were also supported by the rheological measurements, which established the stiffer network of the modified gelators. The stimuli-responsive property was studied by adding various anions to the hydrogels, which revealed that **L₁** gel was a better anion sensor whereas **L₂** gel displayed significant resistance

towards anions. Density functional theory calculations confirmed the increased hydrogen bonding strength of N—H...O vs. N—H...N interactions. This implies that the spatial arrangement of the functional groups and the nature of intermolecular nonbonding interactions of the gelators are crucial for the three-dimensional arrangement of the gel network.

4. Materials and Methods

All starting materials and solvents were purchased from commercial sources and used as supplied. Deionized water was used for all the experiments and anhydrous dichloromethane was obtained by distilling the solvent over CaH₂. The **3-BPU** and **4-BPU** were synthesized following the reported procedure [32] and the analytical data matched with the reported compounds. ¹H and ¹³C NMR spectra were recorded on a Bruker Advance 400 spectrometer (¹H-NMR: 400 MHz, ¹³C-NMR: 100 MHz) and SEM was performed on a Leo Supra 25 microscope.

4.1. Synthesis of the Ligand

4.1.1. 4,4'-(carbonylbis(azanediyl))bis(pyridine 1-oxide) (L₁)

To a solution of **4-BPU** (1.1 g, 5.1 mmol) in DMF (30 mL), 3-chloroperoxybenzoic acid (3.4 g, 14.8 mmol) was added in portions over a period of 15 min at room temperature and the mixture was stirred overnight. The white precipitate obtained was filtered and stirred overnight in 0.05 N HCl. The mixture was filtered, washed with water and dried to obtain **L₁** as a white powder. The product was recrystallized from water. Yield = 0.62 g (2.5 mmol, 49.4%). ¹H-NMR (400 MHz, DMSO-*d*₆): δ = 9.45 (2H, s), 8.10 (4H, d, J = 8.0), 7.49 (4H, d, J = 8.0). ¹³C-NMR (100 MHz, DMSO-*d*₆): δ = 151.47, 138.76, 136.66, 115.25. MS (ESI) m/z for C₁₁H₁₀N₄O₃Na⁺: expected 269.0651, found 269.0663.

4.1.2. 3,3'-(carbonylbis(azanediyl))bis(pyridine 1-oxide) (L₂)

L₂ was synthesized following a similar procedure as above by reacting **3-BPU** (1.1 g, 5.1 mmol) and 3-chloroperoxybenzoic acid (3.4 g, 14.8 mmol) in 30 mL DMF. The product was recrystallized from methanol and all gelation experiments were performed with the recrystallized product. Yield = 0.72 g (2.9 mmol, 56.5%). ¹H-NMR (400 MHz, DMSO-*d*₆): δ = 9.31 (2H, s), 8.53 (2H, d, J = 4.0), 7.92 (2H, m), 7.33–7.34 (4H, m). ¹³C-NMR (100 MHz, DMSO-*d*₆): δ = 151.83, 138.49, 132.88, 129.52, 126.06, 115.45. MS (ESI) m/z for C₁₁H₁₀N₄O₃Na⁺: expected 269.0651, found 269.0659.

4.2. Gelation Studies

4.2.1. Gelation Test

The gelation properties of **L₁** and **L₂** were tested in various solvents by adding 1.0 mL of the solvent to 10.0 mg of *N*-oxide compounds (1.0 wt%) in a standard 7.0 mL vial and the mixture was heated to obtain a clear solution. The solution was sonicated, left undisturbed at room temperature and gelation was confirmed by inversion test. The gelation experiments in a mixed solvent system (1:1, *v/v*) were performed by dissolving the gelator in 500 μL of the appropriate solvent and distilled water (500 μL) was added as cosolvent. The mixture was heated to obtain a clear solution, cooled to room temperature and left undisturbed for gel formation.

4.2.2. Minimum Gel Concentration

The MGC experiment was performed by weighing various amounts of gelator in a standard 7.0 mL vial, followed by adding 1.0 mL of solvent (or solvent mixture). The ligand was dissolved by heating the mixture and the solution was sonicated and left at room temperature for gelation. The minimum concentration at which the gel was obtained after 24 h was recorded as MGC.

4.2.3. T_{gel} Experiments

The gel to solution transition temperature (T_{gel}) was evaluated in different solvent systems using ball-drop method [7,30,44,45]. The required amount of the gelator was dissolved in the solvent or solvent mixtures by heating the mixture in a sealed vial to obtain a clear solution. The solution was cooled to room temperature and after 24 h, a spherical glass ball (52.0 mg) was placed on top of the gel. The vial was placed into an oil bath equipped with a magnetic stirrer and a thermometer. The oil bath was gradually heated and the temperature at which the glass ball touched the bottom of the vial was recorded as T_{gel} .

4.3. Rheology

Rheological measurements were performed in an Anton Paar MCR 302 rheometer using a 25.0 mm stainless steel parallel plate geometry configuration. The **4-BPU**, **L₁**, and **L₂** gels were prepared by dissolving 10.0 mg of the compound in 1.0 mL of water and experiments were performed by scooping a ~1.0 mL portion of gel onto the plate. The **3-BPU** and **L₂** gels were also prepared at 2.5 wt% in EG/water (3:7 *v/v*). Viscoelastic properties were evaluated by oscillatory measurements at a constant temperature of 25.0 °C. Amplitude sweeps were performed with constant frequency (*f*) of 1.0 Hz and log ramp strain (γ) = 0.01–100% and frequency sweeps were carried out between 0.1 and 10.0 Hz within the linear viscoelasticity domain (0.05% strain). The anion sensing experiments were performed by dissolving the mixture of gelator and anions (sodium or potassium salts) in water by heating and sonicating. The mixture was cooled to form gels, the gels were scooped after 24 h, and rheology was performed similarly.

4.4. Scanning Electron Microscopy

The **4-BPU** and **3-BPU** gels were prepared from EG/water (3:7, *v/v*) at 1.0 wt% and 2.5 wt% respectively. The gels of **L₁** (1.0 wt%) and **L₂** (2.5 wt%) were prepared in water and EG/water (3:7, *v/v*), and 1.0 wt% gels were prepared for both **L₁** and **L₂** in DMSO/water (1:1, *v/v*). The resulting gels were filtered after 24 h and dried under a fume hood. A small portion of the dried gels was placed on a pin mount with a carbon tab on top and coated with gold for 2 min. SEM images of the dried gels were analyzed using Leo Supra 25 microscope.

4.5. Single Crystal X-ray Diffraction

X-ray quality single crystals of **3-BPU**, **L₁** and **L₂** were obtained by the slow evaporation of the compounds from corresponding solvents. Needle-shaped crystals of **L₁.H₂O** were obtained by the slow evaporation of an aqueous solution (2.0 mL) of **L₁** (10.0 mg) in an open vial. The crystallization experiment of **L₂** in ethylene glycol was performed by dissolving 20.0 mg of **L₂** in 1.0 mL of EG and left for slow evaporation under the fume hood. Concomitant crystals of block-shaped **L₂.H₂O** and plate shaped **L₂.EG** were obtained in three days. The crystallization experiment performed with **3-BPU** in EG resulted in long needle-shaped crystals in two days, which were obtained by the slow evaporation of 40.0 mg of **3-BPU** in 1.0 mL of ethylene glycol. The crystals were isolated from the solvent and immersed in cryogenic oil before mounting. The crystals were mounted on a Bruker D8 VENTURE (Photon100 CMOS detector) diffractometer equipped with a Cryostream open-flow nitrogen cryostat and the data collection were performed using CuK α radiation ($\lambda = 1.54178 \text{ \AA}$) at 150.0(2) K. The unit cell determination, data collection, data reduction, structure solution/refinement, and empirical absorption correction (SADABS) were carried out using Apex III. The structure was solved by a direct method and refined by the full-matrix least-squares on F^2 for all data using SHELXTL version 2017/1 [48]. All non-disordered nonhydrogen atoms were refined anisotropically, and the hydrogen atoms were placed in the calculated positions and refined using a riding model except for **L₁.H₂O** where the hydrogen atoms of the water molecules were located on the Fourier map and refined. The free variables of disordered carbon atoms in the EG molecule in **3-BPU.2EG** were refined

by the FVAR instruction. The crystallographic data for this paper were deposited at Cambridge Crystallographic Data Centre and the CCDC numbers are 1965865–1965867. These data can be obtained free of charge via www.ccdc.cam.ac.uk/data_request/cif, or by emailing data_request@ccdc.cam.ac.uk.

4.6. X-ray Powder Diffraction

The bulk crystals of L_1 were obtained by the slow evaporation of the solution of L_1 (10.0 mg in 2.0 mL water). The gelator L_2 (20.0 mg) was dissolved in 1.0 mL of EG and left under a fume hood for crystallization resulting in bulk crystals of L_2 . The crystals of 3-BPU were obtained from ethylene glycol solution (40.0 mg in 1.0 mL). The crystals were filtered, dried in the air, and ground to a fine powder. The xerogels of 3-BPU, 4-BPU, L_1 , and L_2 were prepared by filtering the corresponding gels in water or in 3:7 EG/water (*v/v*) mixture at a concentration closer to MGC, followed by drying the residue in a fume hood. XRPD was carried out on the bulk crystals and xerogels using a Bruker D8 Focus instrument.

4.7. Quantum Chemical Calculations

Calculations were performed with the ORCA program, version 4.2.1 [49,50]. The density functional theory-based protocol consisted of the ω B97M–D3BJ functional [51,52] (including the D3 dispersion correction by Grimme and coworkers) [53,54] and the triple-zeta basis set def2–TZVPP [55]. The RIJCOSX [56,57] approximation was used to calculate Coulomb and Exchange integrals, using the def2/J auxiliary basis set by Weigend et al. [58] and the GridX5 (ORCA keyword) grid was used. Tight integration grids for the exchange–correlation terms were also used (Grid5, FinalGrid6 keywords in ORCA). Interaction energies were calculated as electronic energies from relaxed structural optimizations in the gas phase.

Supplementary Materials: The following are available online at <http://www.mdpi.com/2310-2861/6/4/41/s1>, Figure S1: Strain sweep experiments performed on 4-BPU and L_1 gels at 1.0 wt% in water, and 3-BPU and L_2 gels at 2.5 wt% in EG/water (3:7 *v/v*) at 25.0 °C and constant frequency of 1.0 Hz, Figure S2: Frequency sweep experiment performed on 3-BPU and L_2 gels at 2.5 wt% in EG/water (3:7 *v/v*), at 25.0 °C and a constant strain of 0.05%, Figure S3: Xerogels of L_1 obtained from water at 1.0 wt%, Figure S4: Xerogels of L_1 obtained from DMSO/water (1:1 *v/v*) at 1.0 wt%, Figure S5: Xerogels of L_2 obtained from water at 1.0 wt%, Figure S6: Xerogels of L_2 obtained from DMSO/water (1:1 *v/v*) at 1.0 wt%, Figure S7: Comparison of the XRPD pattern of simulated $L_1 \cdot H_2O$, as synthesized and the xerogel from EG/water (3:7 *v/v*) and water at 1.0 wt%, Figure S8: XRPD comparison of simulated $L_2 \cdot EG$, $L_2 \cdot H_2O$, bulk crystals of L_2 , xerogel from EG/water (3:7 *v/v*) at 1.2 wt% and water (1.0 wt%), Figure S9: XRPD comparison of simulated 3-BPU.2EG, 3-BPU, bulk crystals of 3-BPU and xerogels obtained from EG/water (3:7 *v/v*), Figure S10: Frequency sweep experiments performed at 25.0 °C at a constant strain of 0.02% on 4-BPU hydrogel at 1.0 wt%, in presence of three equivalents of anions, Figure S11: Frequency sweep experiments performed at 25.0 °C at a constant strain of 0.02% on L_1 hydrogel at 1.0 wt%, in presence of three equivalents of anions, Figure S12: Frequency sweep experiments performed at 25.0 °C at a constant strain of 0.02% on L_2 hydrogel at 1.0 wt%, in presence of three equivalents of anions, Figure S13: DFT-optimized geometries and calculated interaction energies of various 3-BPU hydrogen-bonding interactions, Figure S14: DFT-optimized geometries and calculated interaction energies of various 4-BPU hydrogen-bonding interactions, Figure S15: DFT-optimized geometries and calculated interaction energies of various L_1 hydrogen-bonding interactions, Figure S16: DFT-optimized geometries and calculated interaction energies of various L_2 hydrogen-bonding interactions. Table S1: Gelation experiment with 4-BPU and 3-BPU in water and 1:1 solvent/water mixture, Table S2: Determination of MGC, Table S3: Crystal data, Table S4: Hydrogen-bonding table.

Author Contributions: Conceptualization, K.K.D. and D.G.; methodology, D.G.; software, R.B.; validation, D.G.; formal analysis, D.G., R.B. and K.K.D.; investigation, D.G.; resources, K.K.D.; data curation, K.K.D.; writing—original draft preparation, K.K.D.; writing—review and editing, D.G., R.B. and K.K.D.; visualization, K.K.D. and D.G.; supervision, K.K.D.; project administration, K.K.D.; funding acquisition, K.K.D. All authors have read and agreed to the published version of the manuscript.

Funding: This research received no external funding.

Acknowledgments: We thank the Science Institute and the University of Iceland Research Fund for financial support. D.G. thanks the University of Iceland Research Fund for Doctoral Research and R.B. thanks the Max Planck Society, Germany for support. We thank Rannis Iceland for Infrastructure grant (150998–0031 & 191763–0031) for a single crystal X-ray diffractometer and Rheometer, Sigurður Sveinn Jonsson, ISOR–Iceland for X-ray powder diffraction analysis and Sigridur Jonsdottir, University of Iceland for NMR and mass spectroscopy.

Conflicts of Interest: The authors declare no conflict of interest.

References

1. Flory, P.J. Introductory lecture. *Faraday Discuss.* **1974**, *57*, 7–18. [[CrossRef](#)]
2. Estroff, L.A.; Hamilton, A.D. Water Gelation by Small Organic Molecules. *Chem. Rev.* **2004**, *104*, 1201–1218. [[CrossRef](#)] [[PubMed](#)]
3. Dastidar, P. Supramolecular gelling agents: Can they be designed? *Chem. Soc. Rev.* **2008**, *37*, 2699–2715. [[CrossRef](#)] [[PubMed](#)]
4. Jones, C.D.; Steed, J.W. Gels with sense: Supramolecular materials that respond to heat, light and sound. *Chem. Soc. Rev.* **2016**, *45*, 6546–6596. [[CrossRef](#)] [[PubMed](#)]
5. Steed, J.W. Anion-tuned supramolecular gels: A natural evolution from urea supramolecular chemistry. *Chem. Soc. Rev.* **2010**, *39*, 3686–3699. [[CrossRef](#)] [[PubMed](#)]
6. Kumar, D.K.; Steed, J.W. Supramolecular gel phase crystallization: Orthogonal self-assembly under non-equilibrium conditions. *Chem. Soc. Rev.* **2014**, *43*, 2080–2088. [[CrossRef](#)]
7. Yu, G.; Yan, X.; Han, C.; Huang, F. Characterization of supramolecular gels. *Chem. Soc. Rev.* **2013**, *42*, 6697–6722. [[CrossRef](#)]
8. Fang, W.; Zhang, Y.; Wu, J.; Liu, C.; Zhu, H.; Tu, T. Recent Advances in Supramolecular Gels and Catalysis. *Chem. Asian J.* **2018**, *13*, 712–729. [[CrossRef](#)]
9. Smith, D.K. Applications of Supramolecular Gels. In *Molecular Gels: Structure and Dynamics*; Weiss, R., Ed.; Royal Society of Chemistry: Cambridge, UK, 2018; pp. 300–371.
10. Foster, J.A.; Damodaran, K.K.; Maurin, A.; Day, G.M.; Thompson, H.P.G.; Cameron, G.J.; Bernal, J.C.; Steed, J.W. Pharmaceutical polymorph control in a drug-mimetic supramolecular gel. *Chem. Sci.* **2017**, *8*, 78–84. [[CrossRef](#)]
11. Lee, K.Y.; Mooney, D.J. Hydrogels for Tissue Engineering. *Chem. Rev.* **2001**, *101*, 1869–1880. [[CrossRef](#)]
12. Van Bommel, K.J.C.; Stuart, M.C.A.; Feringa, B.L.; van Esch, J. Two-stage enzyme mediated drug release from LMWG hydrogels. *Org. Biomol. Chem.* **2005**, *3*, 2917–2920. [[CrossRef](#)] [[PubMed](#)]
13. Yang, X.; Zhang, G.; Zhang, D. Stimuli responsive gels based on low molecular weight gelators. *J. Mater. Chem.* **2012**, *22*, 38–50. [[CrossRef](#)]
14. Meazza, L.; Foster, J.A.; Fucke, K.; Metrangolo, P.; Resnati, G.; Steed, J.W. Halogen-bonding-triggered supramolecular gel formation. *Nat. Chem.* **2013**, *5*, 42–47. [[CrossRef](#)] [[PubMed](#)]
15. Weiss, R.G.; Terech, P. (Eds.) *Molecular Gels: Materials with Self-Assembled Fibrillar Networks*; Springer: Dordrecht, The Netherlands, 2006; p. 978.
16. Steed, J.W. Supramolecular gel chemistry: Developments over the last decade. *Chem. Commun.* **2011**, *47*, 1379–1383. [[CrossRef](#)] [[PubMed](#)]
17. Chivers, P.R.A.; Smith, D.K. Shaping and structuring supramolecular gels. *Nat. Rev. Mater.* **2019**, *4*, 463–478. [[CrossRef](#)]
18. Fages, F.; Voegtle, F.; Zinic, M. Systematic design of amide- and urea-type gelators with tailored properties. *Top. Curr. Chem.* **2005**, *256*, 77–131. [[PubMed](#)]
19. Van Esch, J.; Kellogg, R.M.; Feringa, B.L. Di-urea compounds as gelators for organic solvents. *Tetrahedron Lett.* **1997**, *38*, 281–284. [[CrossRef](#)]
20. Piepenbrock, M.O.M.; Lloyd, G.O.; Clarke, N.; Steed, J.W. Gelation is crucially dependent on functional group orientation and may be tuned by anion binding. *Chem. Commun.* **2008**, 2644–2646. [[CrossRef](#)]
21. Bastiat, G.; Leroux, J.C. Pharmaceutical organogels prepared from aromatic amino acid derivatives. *J. Mater. Chem.* **2009**, *19*, 3867–3877. [[CrossRef](#)]
22. George, M.; Tan, G.; John, V.T.; Weiss, R.G. Urea and Thiourea Derivatives as Low Molecular-Mass Organogelators. *Chem. Eur. J.* **2005**, *11*, 3243–3254. [[CrossRef](#)]
23. Poolman, J.M.; Maity, C.; Boekhoven, J.; van der Mee, L.; le Sage, V.A.A.; Groenewold, G.J.M.; van Kasteren, S.I.; Versluis, F.; van Esch, J.H.; Eelkema, R. A toolbox for controlling the properties and functionalisation of hydrazone-based supramolecular hydrogels. *J. Mater. Chem. B* **2016**, *4*, 852–858. [[CrossRef](#)] [[PubMed](#)]
24. McAulay, K.; Dietrich, B.; Su, H.; Scott, M.T.; Rogers, S.; Al-Hilaly, Y.K.; Cui, H.; Serpell, L.C.; Seddon, A.M.; Draper, E.R.; et al. Using chirality to influence supramolecular gelation. *Chem. Sci.* **2019**, *10*, 7801–7806. [[CrossRef](#)] [[PubMed](#)]

25. Desiraju, G.R. Supramolecular Synthons in Crystal Engineering—A New Organic Synthesis. *Angew. Chem. Int. Ed.* **1995**, *34*, 2311–2327. [[CrossRef](#)]
26. Zurcher, D.M.; Adhia, Y.J.; Romero, J.D.; McNeil, A.J. Modifying a known gelator scaffold for nitrite detection. *Chem. Commun.* **2014**, *50*, 7813–7816. [[CrossRef](#)] [[PubMed](#)]
27. Kumar, D.K.; Jose, D.A.; Dastidar, P.; Das, A. Nonpolymeric Hydrogelators Derived from Trimesic Amides. *Chem. Mater.* **2004**, *16*, 2332–2335. [[CrossRef](#)]
28. Ghosh, D.; Ferfolja, K.; Drabavičius, Ž.; Steed, J.W.; Damodaran, K.K. Crystal habit modification of Cu(ii) isonicotinate–N-oxide complexes using gel phase crystallisation. *New J. Chem.* **2018**, *42*, 19963–19970. [[CrossRef](#)]
29. Kumar, D.K.; Jose, D.A.; Dastidar, P.; Das, A. Nonpolymeric Hydrogelator Derived from N-(4-Pyridyl)isonicotinamide. *Langmuir* **2004**, *20*, 10413–10418. [[CrossRef](#)]
30. Ghosh, D.; Mulvee, M.T.; Damodaran, K.K. Tuning Gel State Properties of Supramolecular Gels by Functional Group Modification. *Molecules* **2019**, *24*, 3472. [[CrossRef](#)]
31. Tomasini, C.; Castellucci, N. Peptides and peptidomimetics that behave as low molecular weight gelators. *Chem. Soc. Rev.* **2013**, *42*, 156–172. [[CrossRef](#)]
32. Kumar, D.K.; Jose, D.A.; Das, A.; Dastidar, P. First snapshot of a nonpolymeric hydrogelator interacting with its gelling solvents. *Chem. Commun.* **2005**, 4059–4061. [[CrossRef](#)]
33. Abraham, S.; Lan, Y.; Lam, R.S.H.; Grahame, D.A.S.; Kim, J.J.H.; Weiss, R.G.; Rogers, M.A. Influence of Positional Isomers on the Macroscale and Nanoscale Architectures of Aggregates of Racemic Hydroxyoctadecanoic Acids in Their Molecular Gel, Dispersion, and Solid States. *Langmuir* **2012**, *28*, 4955–4964. [[CrossRef](#)] [[PubMed](#)]
34. Xu, Y.; Kang, C.; Chen, Y.; Bian, Z.; Qiu, X.; Gao, L.; Meng, Q. In Situ Gel-to-Crystal Transition and Synthesis of Metal Nanoparticles Obtained by Fluorination of a Cyclic β -Aminoalcohol Gelator. *Chem. Eur. J.* **2012**, *18*, 16955–16961. [[CrossRef](#)] [[PubMed](#)]
35. Wang, Y.; Tang, L.; Yu, J. Investigation of Spontaneous Transition from Low-Molecular-Weight Hydrogel into Macroscopic Crystals. *Cryst. Growth Des.* **2008**, *8*, 884–889. [[CrossRef](#)]
36. Braga, D.; d’Agostino, S.; D’Amen, E.; Grepioni, F. Polymorphs from supramolecular gels: Four crystal forms of the same silver(i) supergelator crystallized directly from its gels. *Chem. Commun.* **2011**, *47*, 5154–5156. [[CrossRef](#)]
37. Byrne, P.; Lloyd, G.O.; Applegarth, L.; Anderson, K.M.; Clarke, N.; Steed, J.W. Metal-induced gelation in dipyridyl ureas. *New J. Chem.* **2010**, *34*, 2261–2274. [[CrossRef](#)]
38. Dastidar, P.; Roy, R.; Parveen, R.; Sarkar, K. Supramolecular Synthons Approach in Designing Molecular Gels for Advanced Therapeutics. *Adv. Ther.* **2019**, *2*, 1800061. [[CrossRef](#)]
39. Chandran, S.K.; Nath, N.K.; Cherukuvada, S.; Nangia, A. N–H... N(pyridyl) and N–H... O(urea) hydrogen bonding and molecular conformation of N-aryl-N'-pyridylureas. *J. Mol. Struct.* **2010**, *968*, 99–107. [[CrossRef](#)]
40. Byrne, P.; Turner, D.R.; Lloyd, G.O.; Clarke, N.; Steed, J.W. Gradual Transition from NH...Pyridyl Hydrogen Bonding to the NH...O Tape Synthons in Pyridyl Ureas. *Cryst. Growth Des.* **2008**, *8*, 3335–3344. [[CrossRef](#)]
41. Todd, A.M.; Anderson, K.M.; Byrne, P.; Goeta, A.E.; Steed, J.W. Helical or Polar Guest-Dependent Z' = 1.5 or Z' = 2 Forms of a Sterically Hindered Bis(urea) Clathrate. *Cryst. Growth Des.* **2006**, *6*, 1750–1752. [[CrossRef](#)]
42. Reddy, L.S.; Basavoju, S.; Vangala, V.R.; Nangia, A. Hydrogen Bonding in Crystal Structures of N,N'-Bis(3-pyridyl)urea. Why Is the N–H...O Tape Synthons Absent in Diaryl Ureas with Electron-Withdrawing Groups? *Cryst. Growth Des.* **2006**, *6*, 161–173. [[CrossRef](#)]
43. Ghosh, D.; Lebedyete, I.; Yufit, D.S.; Damodaran, K.K.; Steed, J.W. Selective gelation of N-(4-pyridyl)nicotinamide by copper(ii) salts. *CrystEngComm* **2015**, *17*, 8130–8138. [[CrossRef](#)]
44. Ghosh, D.; Deepa; Damodaran, K.K. Metal complexation induced supramolecular gels for the detection of cyanide in water. *Supramol. Chem.* **2020**, *32*, 276–286. [[CrossRef](#)]
45. Ghosh, D.; Farahani, A.D.; Martin, A.D.; Thordarson, P.; Damodaran, K.K. Unraveling the Self-Assembly Modes in Multicomponent Supramolecular Gels Using Single-Crystal X-ray Diffraction. *Chem. Mater.* **2020**, *32*, 3517–3527. [[CrossRef](#)]
46. Adams, D.J. Does Drying Affect Gel Networks? *Gels* **2018**, *4*, 32. [[CrossRef](#)] [[PubMed](#)]
47. Piepenbrock, M.O.M.; Lloyd, G.O.; Clarke, N.; Steed, J.W. Metal- and Anion-Binding Supramolecular Gels. *Chem. Rev.* **2010**, *110*, 1960–2004. [[CrossRef](#)] [[PubMed](#)]

48. Sheldrick, G.M. Crystal structure refinement with SHELXL. *Acta Crystallogr. Sect. C Cryst. Struct. Chem.* **2015**, *71*, 3–8. [[CrossRef](#)]
49. Neese, F. The ORCA program system. *Wiley Interdiscip. Rev. Comput. Mol. Sci.* **2012**, *2*, 73–78. [[CrossRef](#)]
50. Neese, F. Software update: The ORCA program system, version 4.0. *Wiley Interdiscip. Rev. Comput. Mol. Sci.* **2018**, *8*, e1327. [[CrossRef](#)]
51. Mardirossian, N.; Head-Gordon, M. ω B97M-V: A combinatorially optimized, range-separated hybrid, meta-GGA density functional with VV10 nonlocal correlation. *J. Chem. Phys.* **2016**, *144*, 214110. [[CrossRef](#)]
52. Najibi, A.; Goerigk, L. The Nonlocal Kernel in van der Waals Density Functionals as an Additive Correction: An Extensive Analysis with Special Emphasis on the B97M-V and ω B97M-V Approaches. *J. Chem. Theory Comput.* **2018**, *14*, 5725–5738. [[CrossRef](#)]
53. Grimme, S.; Antony, J.; Ehrlich, S.; Krieg, H. A consistent and accurate ab initio parametrization of density functional dispersion correction (DFT-D) for the 94 elements H-Pu. *J. Chem. Phys.* **2010**, *132*, 154104. [[CrossRef](#)] [[PubMed](#)]
54. Grimme, S.; Ehrlich, S.; Goerigk, L. Effect of the damping function in dispersion corrected density functional theory. *J. Comput. Chem.* **2011**, *32*, 1456–1465. [[CrossRef](#)] [[PubMed](#)]
55. Weigend, F.; Ahlrichs, R. Balanced basis sets of split valence, triple zeta valence and quadruple zeta valence quality for H to Rn: Design and assessment of accuracy. *Phys. Chem. Chem. Phys.* **2005**, *7*, 3297–3305. [[CrossRef](#)]
56. Neese, F.; Wennmohs, F.; Hansen, A.; Becker, U. Efficient, approximate and parallel Hartree–Fock and hybrid DFT calculations. A ‘chain-of-spheres’ algorithm for the Hartree–Fock exchange. *Chem. Phys.* **2009**, *356*, 98–109. [[CrossRef](#)]
57. Izsák, R.; Neese, F. An overlap fitted chain of spheres exchange method. *J. Chem. Phys.* **2011**, *135*, 144105. [[CrossRef](#)] [[PubMed](#)]
58. Weigend, F. Accurate Coulomb-fitting basis sets for H to Rn. *Phys. Chem. Chem. Phys.* **2006**, *8*, 1057–1065. [[CrossRef](#)]

Publisher’s Note: MDPI stays neutral with regard to jurisdictional claims in published maps and institutional affiliations.



© 2020 by the authors. Licensee MDPI, Basel, Switzerland. This article is an open access article distributed under the terms and conditions of the Creative Commons Attribution (CC BY) license (<http://creativecommons.org/licenses/by/4.0/>).